Parametric Analyses of Multispan Viscoelastic Shear Deformable Beams Under Excitation of a Moving Mass

Keivan Kiani[1]
e-mail: k_kiani@civil.sharif.edu

Ali Nikkhoo
e-mail: nikkhoo@civil.sharif.edu

Department of Civil Engineering,
Sharif University of Technology,
Azadi Ave.,
Tehran, Iran, P.O. Box 11365-9313

Bahman Mehri
Department of Mathematical Sciences,
Sharif University of Technology,
Tehran, Iran 11365-9415
e-mail: mehri@sharif.edu

This paper presents a numerical parametric study on design parameters of multispan viscoelastic shear deformable beams subjected to a moving mass via generalized moving least squares method (GMLSM). For utilizing Lagrange's equations, the unknown parameters of the problem are stated in terms of GMLSM shape functions and the generalized Newmark-β scheme is applied for solving the discrete equations of motion in time domain. The effects of moving mass weight and velocity, material relaxation rate, slenderness, and span number of the beam on the design parameters and possibility of mass separation from the base beam are scrutinized in some detail. The results reveal that for low values of beam slenderness, the Euler–Bernoulli beam theory or even Timoshenko beam theory could not predict the real dynamic behavior of the multispan viscoelastic beam properly. Moreover, higher beam span number would result in higher inertial effects as well as design parameters values. Also, more distinction has been observed between the predicted values of design parameters regarding the shear deformable beams and those of Euler–Bernoulli beams, specifically for high levels of moving mass velocity and low values of material relaxation rate. Furthermore, the possibility of mass separation from the base beam moves to a greater extent as the beam span number increases and the relaxation rate of the beam material decreases, regardless of the assumed beam theory. [DOI: 10.1115/1.3147165]

1 Introduction

Vibration of beam structures acted upon by moving loads (or masses) has been investigated theoretically and experimentally due to its importance and complexity over the past century. As mass passes over a beam, it exerts a time variant force on the beam because of the induced inertial effects of the moving load [1–4]. Actually, the applied force is mainly affected by the beam motion, in which the latter one is a function of existing boundary conditions of the beam as well as the assumed beam theory [5]. The need to reduce the effects of the applied force, especially in important structures under moving masses, is a hot topic among the mechanical and structural engineers. Vibration reduction techniques are commonly placed into two categories: active and passive vibration reductions. The latter one is the most widely used since it is the simplest, most effective, and economical solution in practical applications. One famous passive device is the constrained layer viscoelastic laminated tuned mass damper utilized as a capable means for decreasing unwanted resonant vibrations in the structures such as decks of aircraft carriers, long span bridges, and continuous pipelines conveying fluid. In all of these applications, if the host structure is controlled thoroughly by the aforementioned passive system, the structural system could be modeled as a viscoelastic multispan beam-plate under external loading.

On the other hand, beam-like structures used in real practice may have sizable thickness or high ratio of the shear modulus to the longitudinal one. In such cases, the transverse shear and rotatory inertia could not be neglected as assumed in the theory of thin beams. As a result, the thick beam models based on the Timoshenko or other higher-order shear deformable beam theories have gained more popularity in analyzing the mentioned structures, particularly when capturing higher natural frequencies is of concern.

A few studies have been carried out with regard to the vibration analysis of multispan beams subjected to the moving masses. Frýba [1] presented analytical solutions in some special cases for the problems of Euler–Bernoulli beam structures (single and multispan beams) subjected to a system of moving loads or masses. To elaborate the effect of shear and rotatory inertia, he demonstrated an analytical solution for a simply supported Timoshenko beam excited by a moving load. Lee [6] explored the dynamic response of a simply supported Timoshenko beam subjected to a moving mass, using assumed mode method. He also investigated the possibility of moving mass separation from the base beam due to the inertial effects of the moving load. This was detected by monitoring the contact force between the base beam and the moving mass.

The problem of multispan Euler–Bernoulli beams traversed by moving loads is fairly well studied in the past 2 decades, employing miscellaneous methodologies [1,7–10]. In this regard, a few works are available in the literature as the effects of the moving load inertia are taken into consideration in the mathematical formulation of the problem. Using the eigenfunction expansion method, Ichikawa et al. [11] explored the dynamic response of multispan Euler–Bernoulli beam acted upon by a moving mass. It was elucidated that the effects of moving load inertia substantially influence the vibration behavior of the system, especially for high values of moving mass weight and velocity.

Toshiaki and Kenichi [12] studied the dynamic behavior of classical Timoshenko and Levinson beams under moving loads with spring and damping by using transfer matrix method. The accuracy of the proposed models and dynamic responses of multispan beams was demonstrated through several numerical results. Wang [13] investigated vibration of multispan Timoshenko beams under a moving force by modal analysis. The effects of span number, rotatory inertia, and shear deformation on design parameters

[1]Corresponding author.

Contributed by the Technical Committee on Vibration and Sound of ASME for publication in the Journal of Vibration and Acoustics. Manuscript received November 1, 2008; final manuscript received April 10, 2009; published online September 16, 2009. Assoc. Editor: Massimo Ruzzene.

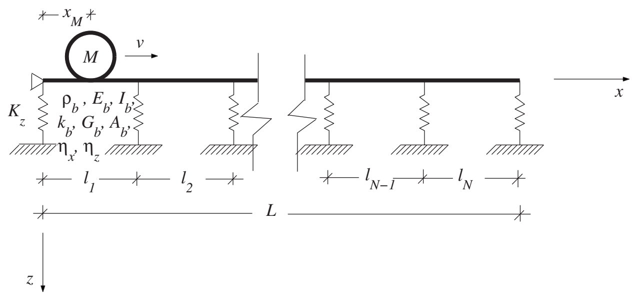

Fig. 1 Schematic representation of a multispan viscoelastic shear deformable beam subjected to a moving mass

of the beam were examined. It was indicated that higher span number would result in higher values of design parameters. In another work, Wang and Tsu [14] explored the out-of-plane vibration of a multispan Timoshenko curved beam due to a moving load including the warping inertia of the beam by modal analysis. It was shown that a critical velocity exists at which the absolutely maximum strain energy density of the curved beam occurs; additionally, higher span number results in higher absolute maximum strain energy density and critical velocity of the beam. The dynamic behavior of a continuous nonuniform Timoshenko beam subjected to a set of moving loads was studied by Zhu and Law [15] based on Hamilton's principle in which the intermediate supports were modeled by very stiff linear springs.

A parametric study on the evaluation of design parameters including maximum deflection and bending moment of beam structures subjected to a moving mass was conducted by Kiani et al. [5] via reproducing kernel particle method (RKPM). The results manifested that according to the slenderness and boundary conditions of the beam, the appropriate beam theory should be selected for precise capturing of the beam dynamic response. This noteworthy issue inspired the authors to explore the dynamic behavior of multispan viscoelastic shear deformable beams, which are traversed by a moving mass. Therefore, this work is devoted to the assessment of design parameters for multispan viscoelastic Timoshenko and higher-order beams under the excitation of a moving mass by utilizing GMLSM. This meshless numerical method was developed by Atluri et al. [16] through modifying the local approximation in the moving least squares method by adding the first derivative of the unknown field as an independent variable. Besides, static analyses of thin beams based on GMLSM revealed remarkable results for both deflection and bending moment of thin beams with different boundary conditions [16]. For using Lagrange's equations, the unknown parameters of the problem are discretized according to the so-called meshless method. Then, the generalized Newmark-β scheme is employed for solving discrete equations of motion in time domain based on the work of Kiani et al. [5]. The maximum values of deflection plus maximum positive and negative bending moments are considered as the crucial design parameters. The effects of moving mass weight and velocity, material relaxation rate, slenderness, and span number of the base beam on the design parameters are studied in some detail for the multispan viscoelastic Euler–Bernoulli beam (EB), Timoshenko beam (TB), and higher-order beam (HOB). The validity of the calculations is corroborated by comparing the obtained results of the proposed model with those of other researchers.

2 Assumptions of the Mechanical Problem

The under study system is a finite NS-span beam with length L transversely constrained at support locations by axial linear springs with constant K_z, as depicted in Fig. 1. The beam is also axially fixed in one end. The length of the ith span of the beam is l_i and in the case of equal span lengths, $l_i=L/NS$; $i=1,2,\ldots,NS$. The elastic field components of the system are outlined in the Cartesian coordinate system, with the x-axis coincident to the neutral axis of the undeformed beam, and the z-axis perpendicular to the beam neutral axis toward the applied gravitational acceleration, g. In the modeling of the problem, the following assumptions are made. (1) The material of the beam is linear viscoelastic isotropic homogeneous with elastic modulus of E_b and viscosity values of η_x and η_z in the x and z directions, respectively. The material behavior of the beam obeys Kelvin–Voigt model with the relaxation rates of $\lambda_x=\eta_x/E_b$ and $\lambda_z=\eta_z/E_b$, which are assumed to be age independent. (2) The cross-section area of the beam, A_b, and the beam density, ρ_b, are uniform along the beam. (3) At the time $t=0$, the moving mass M enters the left hand end of the beam with constant velocity v. The only applied load is due to the normal contact force of the moving mass on the beam. Furthermore, the moving mass would be in contact with the beam at all times. (4) The only acceleration component for the moving mass over the supposed beam is $\ddot{u}_{zM}=(\ddot{u}_z+2v\dot{u}_{z,x}+v^2u_{z,xx})_{x=x_M}$, where $u_z=u_z(x,z,t)$ denotes the transverse displacement component of the beam.

3 The Numerical Solution via GMLSM

In the fourth-order boundary value problems such as thin beam problems, it would be necessary to impose both displacement and its slope conditions at the same point in the computational domain. Due to this necessity, the conventional moving least squares method was generalized by Atluri et al. [16], utilizing the meshless interpolation scheme for the meshless local Petrov–Galerkin method. In this regard, the slopes of the variable fields are introduced as independent variables by generalizing the local approximation in the moving least squares method. This innovative method was introduced as GMLSM. In the remainder of this part, construction of the GMLSM shape functions and their first and second derivatives for one-dimensional domain will be explained in some detail. Subsequently, the application of GMLSM for solving the problem of multispan viscoelastic TB and HOB subjected to a moving mass will be outlined.

3.1 Construction of GMLSM Shape Functions and Their Derivatives. Consider a continuous function $u(x)$ defined on a one-dimensional domain Ω, where the nodal values and its derivative at the distinct points $x_I(1\leq I\leq NP;\ NP=\text{number of particles})$ are given as $\hat{u}_I^{(0)}$ and $\hat{u}_I^{(1)}$, in which $\hat{u}_I^{(0)}=u(x_I)$, $\hat{u}_I^{(1)}=(d/dx)u(x_I)$. For each point $\bar{x}\in\Omega$, one may assume a local approximation $u_{\bar{x}}(x)$ in a proper small neighborhood of $x=\bar{x}$ as

$$u(x)\approx u_{\bar{x}}(x)=\mathbf{p}^T(x-\bar{x})\mathbf{b}(\bar{x}) \tag{1}$$

in which $\mathbf{p}^T$ is a polynomial bases vector and $\mathbf{b}(\bar{x})$ is the vector of unknown coefficients. For instance, the mth-order polynomial in one-dimensional domain is expressed as $\mathbf{p}^T(x)=[1,x,x^2,\ldots,x^m]$. In contrast to Ref. [16], the vector parameter $\mathbf{p}^T$ is expressed in a local coordinate system about $x=\bar{x}$. This simple improvement vanishes numerical instabilities due to the generation of possibly large numbers in the next matrices. The first derivative of the local approximation $u_{\bar{x}}(x)$ is readily obtained as

$$u_{,x}(x)\approx\frac{d}{dx}u_{\bar{x}}(x)=\frac{d}{dx}\mathbf{p}^T(x-\bar{x})\mathbf{b}(\bar{x}) \tag{2}$$

in which $(d/dx)\mathbf{p}^T(x-\bar{x})=[0,1,2(x-\bar{x}),3(x-\bar{x})^2,\ldots,m(x-\bar{x})^{m-1}]$ for the mth-order polynomial bases vector. The coefficient vector $\mathbf{b}(\bar{x})$ is determined such that it minimizes the following [16]:

$$J_{\bar{x}}(\mathbf{b})=\sum_{I=1}^{NP}\left\{w_I^{(0)}(\bar{x})[u_{\bar{x}}(x)-\hat{u}_I^{(0)}]^2+w_I^{(1)}(\bar{x})\left[\frac{d}{dx}u_{\bar{x}}(x)-\hat{u}_I^{(1)}\right]^2\right\} \tag{3}$$

where $w_I^{(0)}$ and $w_I^{(1)}$ are the appropriate weight functions associated with the Ith point (i.e., particle) of the spatial domain. Substituting Eqs. (1) and (2) into Eq. (3) leads to

$$J_{\bar{x}}(\mathbf{b})=\sum_{I=1}^{NP}\left\{w_I^{(0)}(\bar{x})[\mathbf{p}^T(x_I-\bar{x})\mathbf{b}-\hat{u}_I^{(0)}]^2+w_I^{(1)}(\bar{x})\left[\frac{d}{dx}\mathbf{p}^T(x_I-\bar{x})\mathbf{b}-\hat{u}_I^{(1)}\right]^2\right\} \tag{4}$$

or in matrix form

$$J_{\bar{x}}(\mathbf{b})=[\mathbf{Pb}-\hat{\mathbf{u}}^{(0)}]^T\mathbf{W}^{(0)}(\bar{x})[\mathbf{Pb}-\hat{\mathbf{u}}^{(0)}]+[\mathbf{P}_{,x}\mathbf{b}-\hat{\mathbf{u}}^{(1)}]^T\mathbf{W}^{(1)}(\bar{x})[\mathbf{P}_{,x}\mathbf{b}-\hat{\mathbf{u}}^{(1)}] \tag{5}$$

where

$$\begin{gathered}
\mathbf{P}=[\mathbf{p}(x_1-\bar{x}),\mathbf{p}(x_2-\bar{x}),\ldots,\mathbf{p}(x_{NP-\bar{x}})]^T\\
\mathbf{P}_{,x}=\left[\frac{\partial\mathbf{p}(x_1-\bar{x})}{\partial x},\frac{\partial\mathbf{p}(x_2-\bar{x})}{\partial x},\ldots,\frac{\partial\mathbf{p}(x_{NP}-\bar{x})}{\partial x}\right]^T\\
\mathbf{u}^{(n)}=[u^{(n)}(x_1),u^{(n)}(x_2),\ldots,u^{(n)}(x_{NP})]^T;\quad n=0,1\\
[\mathbf{W}^{(n)}(\bar{x})]_{IJ}=w_I^{(n)}(\bar{x})\delta_{IJ};\quad I,J=1,2,\ldots,NP
\end{gathered} \tag{6}$$

in which δ_{IJ} is the Kroneker delta, and there is no summation on I. The stationary condition of $J_{\bar{x}}(\mathbf{b})$ with respect to the vector $\mathbf{b}$ requires that

$$\mathbf{A}(\bar{x})\mathbf{b}=\mathbf{C}^{(0)}\hat{\mathbf{u}}^{(0)}+\mathbf{C}^{(1)}\hat{\mathbf{u}}^{(1)} \tag{7}$$

where

$$\begin{gathered}
\mathbf{A}(\bar{x})=\mathbf{P}^T\mathbf{W}^{(0)}\mathbf{P}+\mathbf{P}_{,x}^T\mathbf{W}^{(1)}\mathbf{P}_{,x}\\
\mathbf{C}^{(n)}=\mathbf{P}^T\mathbf{W}^{(n)};\quad n=0,1
\end{gathered} \tag{8}$$

Solving for $\mathbf{b}$ from Eq. (7) and substituting it into Eq. (1) leads to

$$u(\bar{x})\approx\sum_{n=0}^{1}\tilde{\boldsymbol{\Phi}}^{(k)}(\bar{x})\mathbf{u}^{(n)}=\sum_{n=0}^{1}\sum_{I=1}^{NP}\phi_I^{(n)}(\bar{x})u_I^{(n)} \tag{9}$$

in which

$$\tilde{\boldsymbol{\Phi}}^{(n)}(\bar{x})=\mathbf{p}^T(0)\mathbf{A}^{-1}\mathbf{P}^T\mathbf{W}^{(n)};\quad n=0,1 \tag{10}$$

or

$$\phi_I^{(n)}=\sum_{k=1}^{m}\sum_{L=1}^{NP}\sum_{j=1}^{m}\mathbf{p}_j^T(0)\mathbf{A}_{jk}^{-1}\mathbf{P}_{Lk}\mathbf{W}_{LI}^{(n)} \tag{11}$$

where $\phi_I^{(n)}$ is the $(n+1)$th kind of the GMLSM shape function associated with the Ith particle. The first and second derivatives of the GMLSM shape functions are required for the computations. Consequently, one can obtain

$$\phi_{I,x}^{(n)}=\sum_{k=1}^{m}\sum_{L=1}^{NP}\sum_{j=1}^{m}\mathbf{p}_j^T(0)[\mathbf{A}_{,x_{jk}}^{-1}\mathbf{P}_{Lk}\mathbf{W}_{LI}^{(n)}+\mathbf{A}_{jk}^{-1}\mathbf{P}_{,x_{Lk}}\mathbf{W}_{LI}^{(n)}+\mathbf{A}_{jk}^{-1}\mathbf{P}_{Lk}\mathbf{W}_{,x_{LI}}^{(n)}] \tag{12}$$

and

$$\phi_{I,xx}^{(n)}=\sum_{k=1}^{m}\sum_{L=1}^{NP}\sum_{j=1}^{m}\mathbf{p}_j^T(0)\left[\begin{matrix}\mathbf{A}_{,xx_{jk}}^{-1}\mathbf{P}_{Lk}\mathbf{W}_{LI}^{(n)}+2\mathbf{A}_{,x_{jk}}^{-1}\mathbf{P}_{,x_{Lk}}\mathbf{W}_{LI}^{(n)}+2\mathbf{A}_{,x_{jk}}^{-1}\mathbf{P}_{Lk}\mathbf{W}_{,x_{LI}}^{(n)}+\\ \mathbf{A}_{jk}^{-1}\mathbf{P}_{,xx_{Lk}}\mathbf{W}_{LI}^{(n)}+2\mathbf{A}_{jk}^{-1}\mathbf{P}_{,x_{Lk}}\mathbf{W}_{,x_{LI}}^{(n)}+\mathbf{A}_{jk}^{-1}\mathbf{P}_{Lk}\mathbf{W}_{,xx_{LI}}^{(n)}\end{matrix}\right] \tag{13}$$

The values of $\mathbf{A}_{,x}^{-1}$ and $\mathbf{A}_{,xx}^{-1}$ can be calculated by taking once and twice differentiation from the equation $\mathbf{A}^{-1}\mathbf{A}=\mathbf{I}$, in which $\mathbf{I}$ is the identity matrix. In this paper, the utilized weight function for both kinds of GMLSM shape functions is a third-order spline function (i.e., cubic spline) as

$$w_I^{(n)}(x)=\begin{cases}\frac{2}{3}-4|z|^2+4|z|^3, & 0\le|z|\le\frac{1}{2},\ n=0,1\\ \frac{4}{3}-4|z|+4|z|^2-\frac{4}{3}|z|^3, & \frac{1}{2}\le|z|\le 1,\ n=0,1\end{cases} \tag{14}$$

in which $z=(x-x_I)/a_I$, where the parameter a_I denotes the influence domain radius of the weight function associated with the Ith particle.

3.2 Governing Equations of Motion for Multispan Viscoelastic TB. Let $u_z=w(x,t)$ and $\theta=\theta(x,t)$ correspond to the transverse displacement and cross-section angle of the beam, respectively. Therefore, the longitudinal displacement is $u_x=-z\theta(x,t)$. For the case of small displacement, the strain components are expressed as $\epsilon_{xx}=-z\theta_{,x}$ and $\gamma_{xz}=w_{,x}-\theta$, so the nonzero components of stress field are $\sigma_{xx}=E\epsilon_{xx}+\eta_x\dot{\epsilon}_{xx}$ and $\sigma_{xz}=G\gamma_{xz}+\eta_z\dot{\gamma}_{xz}$. Subsequently, the resultant shear force (Q_T) and bending moment (M_T) within the beam can be written as

$$\begin{gathered}
Q_T=\int_A\sigma_{xz}dA=k_b[G_bA_b(\dot{w}_{,x}-\theta)+\eta_zA_b(\dot{w}_{,x}-\dot{\theta})]\\
M_T=\int_A\sigma_{xx}zdA=-(E_bI_b\theta_{,x}+\eta_xI_b\dot{\theta}_{,x})
\end{gathered} \tag{15}$$

where k_b is the shear correction factor of the Timoshenko beam. The Lagrangian functional is defined as

$$L=T-(U+V) \tag{16}$$

in which T is the kinetic energy, U is the elastic strain energy, and V is the potential energy of the beam and spring system subjected to a moving mass loading. These parameters are expressed as

$$T=\frac{1}{2}\int_0^L\rho_b(I_b\dot{\theta}^2+A_b\dot{w}^2)dx \tag{17}$$

$$U=\frac{1}{2}\int_0^L[E_bI_b\theta_{,x}^2+k_bG_bA_b(w_{,x}-\theta)^2]dx+\frac{1}{2}\int_{\Gamma_b}K_zw^2d\Gamma \tag{18}$$

$$V=-\int_0^LM[g-(\ddot{w}+2v\dot{w}_{,x}+v^2w_{,xx})]w\delta(x-x_M)H(L-x_M)dx \tag{19}$$

in which Γ_b denotes the constrained boundary of the beam domain, I_b is the second moment inertia of the beam, and $\delta(x)$ and $H(x)$ are the Dirac-delta function and the Heaviside step function. Furthermore, the dissipation function due to existing damping within the beam structure is given by

$$R=\frac{1}{2}\int_0^L[\eta_xI_b\dot{\theta}_{,x}^2+k_b\eta_zA_b(\dot{w}_{,x}-\dot{\theta})^2]dx \tag{20}$$

According to spatial discretization via GMLSM, the unknowns of the one-dimensional problem could be discretized as

$$w(x,t)=\mathbf{\Phi}_I^T\mathbf{w}_I=\mathbf{w}_I^T\mathbf{\Phi}_I;\quad I=1,2,\ldots,NP$$
$$\theta(x,t)=\mathbf{\Phi}_I^T\mathbf{\Theta}_I=\mathbf{\Theta}_I^T\mathbf{\Phi}_I \tag{21}$$

in which

$$\mathbf{\Phi}_I^T=[\phi_I^{(0)},\phi_I^{(1)}],\quad \mathbf{w}_I^T=[w_I^{(0)},w_I^{(1)}],\quad \mathbf{\Theta}_I^T=[\theta_I^{(0)},\theta_I^{(1)}] \tag{22}$$

where I is the free index, NP is the number of particles, and $w_I^{(l)}$ and $\theta_I^{(l)}$ are the nodal parameter values of the unknowns w and θ associated with the Ith particle, correspondingly. Substituting Eq. (21) into Eqs. (17)–(20) and utilizing the Lagrange's equations as

$$\frac{\partial L}{\partial w_I^{(l)}}-\frac{d}{dt}\frac{\partial L}{\partial \dot{w}_I^{(l)}}-\frac{\partial R}{\partial \dot{w}_I^{(l)}}=0,\quad l=1,2$$
$$\frac{\partial L}{\partial \theta_I^{(l)}}-\frac{d}{dt}\frac{\partial L}{\partial \dot{\theta}_I^{(l)}}-\frac{\partial R}{\partial \dot{\theta}_I^{(l)}}=0 \tag{23}$$

the following set of equations of motion could be obtained:

$$\mathbf{M}_b\ddot{\mathbf{x}}+\mathbf{C}_b\dot{\mathbf{x}}+\mathbf{K}_b\mathbf{x}=\mathbf{f}_b \tag{24}$$

where

$$\mathbf{M}_b=\begin{bmatrix}\mathbf{M}_b^{ww} & \mathbf{M}_b^{w\theta}\\ \mathbf{M}_b^{\theta w} & \mathbf{M}_b^{\theta\theta}\end{bmatrix},\quad \mathbf{C}_b=\begin{bmatrix}\mathbf{C}_b^{ww} & \mathbf{C}_b^{w\theta}\\ \mathbf{C}_b^{\theta w} & \mathbf{C}_b^{\theta\theta}\end{bmatrix},\quad \mathbf{K}_b=\begin{bmatrix}\mathbf{K}_b^{ww} & \mathbf{K}_b^{w\theta}\\ \mathbf{K}_b^{\theta w} & \mathbf{K}_b^{\theta\theta}\end{bmatrix}$$
$$\mathbf{f}_b=\begin{Bmatrix}\mathbf{f}_b^w\\ \mathbf{f}_b^\theta\end{Bmatrix},\quad \mathbf{x}_J=\begin{Bmatrix}\mathbf{w}_J(t)\\ \mathbf{\Theta}_J(t)\end{Bmatrix} \tag{25}$$

in which the appropriate submatrices are defined as

$$[\mathbf{M}_b^{ww}]_{IJ}=\int_0^L \rho_bA_b\mathbf{\Phi}_I\mathbf{\Phi}_J^Tdx+M\mathbf{\Phi}_I(x_M)\mathbf{\Phi}_J^T(x_M)H(L-x_M) \tag{26}$$

$$[\mathbf{M}_b^{\theta\theta}]_{IJ}=\int_0^L \rho_bI_b\mathbf{\Phi}_I\mathbf{\Phi}_J^Tdx \tag{27}$$

$$[\mathbf{C}_b^{ww}]_{IJ}=\int_0^L k_b\eta_zA_b\mathbf{\Phi}_{I,x}\mathbf{\Phi}_{J,x}^Tdx+2Mv\mathbf{\Phi}_I(x_M)\mathbf{\Phi}_{J,x}^T(x_M)H(L-x_M) \tag{28}$$

$$[\mathbf{C}_b^{w\theta}]_{IJ}=-\int_0^L k_b\eta_zA_b\mathbf{\Phi}_{I,x}\mathbf{\Phi}_J^Tdx \tag{29}$$

$$[\mathbf{C}_b^{\theta w}]_{IJ}=-\int_0^L k_b\eta_zA_b\mathbf{\Phi}_I\mathbf{\Phi}_{J,x}^Tdx \tag{30}$$

$$[\mathbf{C}_b^{\theta\theta}]_{IJ}=\int_0^L (k_b\eta_zA_b\mathbf{\Phi}_I\mathbf{\Phi}_J^T+\eta_xI_b\mathbf{\Phi}_{I,x}\mathbf{\Phi}_{J,x}^T)dx \tag{31}$$

$$[\mathbf{K}_b^{ww}]_{IJ}=\int_0^L k_bG_bA_b\mathbf{\Phi}_{I,x}\mathbf{\Phi}_{J,x}^Tdx+\int_{\Gamma_b}K_z\mathbf{\Phi}_I\mathbf{\Phi}_J^Td\Gamma+Mv^2\mathbf{\Phi}_I(x_M)\mathbf{\Phi}_{J,xx}^T(x_M)H(L-x_M) \tag{32}$$

$$[\mathbf{K}_b^{w\theta}]_{IJ}=-\int_0^L k_bG_bA_b\mathbf{\Phi}_{I,x}\mathbf{\Phi}_J^Tdx \tag{33}$$

$$[\mathbf{K}_b^{\theta w}]_{IJ}=-\int_0^L k_bG_bA_b\mathbf{\Phi}_I\mathbf{\Phi}_{J,x}^Tdx \tag{34}$$

$$[\mathbf{K}_b^{\theta\theta}]_{IJ}=\int_0^L (k_bG_bA_b\mathbf{\Phi}_I\mathbf{\Phi}_J^T+E_bI_b\mathbf{\Phi}_{I,x}\mathbf{\Phi}_{J,x}^T)dx \tag{35}$$

$$[\mathbf{f}_b^w]_I=Mg\mathbf{\Phi}_I(x_M)H(L-x_M) \tag{36}$$

3.3 Governing Equations of Motion for Multispan Viscoelastic HOB. Assume a HOB with constant transverse deformation across its thickness as $u_z=w(x,t)$, and the longitudinal displacement of the beam as $u_x=x\psi-\alpha z^3(\psi+w_{,x})$ [17], in which $\alpha=4/(3h^2)$ (h is the thickness of the beam) and ψ is the deflection angle of the cross section of the beam with reference to the undeformed plane about the y-axis. In the case of small deformation, the nonzero strain components are $\epsilon_{xx}=z\psi_{,x}-\alpha z^3(\psi_{,x}+w_{,xx})$ and $\gamma_{xz}=(1-3\alpha z^2)(\psi+w_{,x})$. Based on the elastic Kelvin–Voigt material behavior, the stress-strain relations are analogous to those mentioned in Sec. 3.2 for TB. As a result, the resultant shear force and bending moment of a HOB can be written as

$$Q_H=\kappa(\psi+w_{,x})+\chi(\dot{\psi}+\dot{w}_{,x})$$
$$M_H=J_2\psi_{,x}-\alpha J_4(\psi_{,x}+w_{,xx})+P_2\dot{\psi}_{,x}-\alpha P_4(\dot{\psi}_{,x}+\dot{w}_{,xx}) \tag{37}$$

in which

$$J_n=\int_A Ez^ndA;\quad n=2,4,6$$
$$P_n=\int_A \eta_xz^ndA \tag{38}$$

and

$$\kappa=G_b(A_b-3\alpha I_b)$$
$$\chi=\eta_z(A_b-3\alpha I_b) \tag{39}$$

Moreover, components of the total energy (L) and dissipation function (R) are derived as the following:

$$T=\frac{1}{2}\int_0^L[I_0\dot{w}_{,x}^2+I_2\dot{\psi}^2-2\alpha I_4\dot{\psi}(\dot{\psi}+\dot{w}_{,x})+\alpha^2I_6(\dot{\psi}+\dot{w}')^2]dx \tag{40}$$

$$U=\frac{1}{2}\int_0^L[J_2\psi_{,x}^2-2\alpha J_4\psi_{,x}(\psi_{,x}+w_{,xx})+\kappa(\psi+w_{,x})^2+\alpha^2J_6(\Psi_{,x}+w_{,xx})^2]dx+\frac{1}{2}\int_{\Gamma_b}K_zw^2d\Gamma \tag{41}$$

$$V=-\int_0^L M[g-(\ddot{w}+2v\dot{w}_{,x}+v^2w_{,xx})]w\delta(x-x_M)H(L-x_M)dx \tag{42}$$

$$R=\frac{1}{2}\int_0^L[P_2\dot{\psi}_{,x}^2-2\alpha P_4\dot{\psi}_{,x}(\dot{\psi}_{,x}+\dot{w}_{,xx})+\kappa(\dot{\psi}+\dot{w}_{,x})^2+\alpha^2P_6(\dot{\psi}_{,x}+\dot{w}_{,xx})^2]dx \tag{43}$$

Assuming $\psi(x,t)=\mathbf{\Phi}_I^T(x)\Psi_I(t)$, $I=1,2,\ldots,NP$ in which $\Psi_I^T(t)=[\psi_I^{(0)}(t),\psi_I^{(1)}(t)]$, and substituting spatial discretized form of w and ψ into Eqs. (40)–(43), Lagrange's equations are implemented (as mentioned in Sec. 3.2) which leads to the set of equations of motion as

$$\mathbf{M}_b\ddot{\mathbf{x}} + \mathbf{C}_b\dot{\mathbf{x}} + \mathbf{K}_b\mathbf{x} = \mathbf{f}_b \tag{44}$$

in which

$$\mathbf{M}_b = \begin{bmatrix} \mathbf{M}_b^{ww} & \mathbf{M}_b^{w\psi} \\ \mathbf{M}_b^{\psi w} & \mathbf{M}_b^{\psi\psi} \end{bmatrix}, \quad \mathbf{C}_b = \begin{bmatrix} \mathbf{C}_b^{ww} & \mathbf{C}_b^{w\psi} \\ \mathbf{C}_b^{\psi w} & \mathbf{C}_b^{\psi\psi} \end{bmatrix}, \quad \mathbf{K}_b = \begin{bmatrix} \mathbf{K}_b^{ww} & \mathbf{K}_b^{w\psi} \\ \mathbf{K}_b^{\psi w} & \mathbf{K}_b^{\psi\psi} \end{bmatrix}$$

$$\mathbf{f}_b = \begin{Bmatrix} \mathbf{f}_b^{w} \\ \mathbf{f}_b^{\psi} \end{Bmatrix}, \quad \mathbf{x}_J = \begin{Bmatrix} \mathbf{w}_J(t) \\ \mathbf{\Psi}_J(t) \end{Bmatrix} \tag{45}$$

where the appropriate submatrices are defined as

$$[\mathbf{M}_b^{ww}]_{IJ} = \int_0^L (I_0\mathbf{\Phi}_I\mathbf{\Phi}_J^T + \alpha^2 I_6\mathbf{\Phi}_{I,xx}\mathbf{\Phi}_{J,xx}^T)dx + M\mathbf{\Phi}_I(x_M)\mathbf{\Phi}_J^T(x_M)H(L-x_M) \tag{46}$$

$$[\mathbf{M}_b^{w\psi}]_{IJ} = \int_0^L (-\alpha I_4\mathbf{\Phi}_{I,x}\mathbf{\Phi}_J^T + \alpha^2 I_6\mathbf{\Phi}_{I,x}\mathbf{\Phi}_J^T)dx \tag{47}$$

$$[\mathbf{M}_b^{\psi w}]_{IJ} = \int_0^L (-\alpha I_4\mathbf{\Phi}_I\mathbf{\Phi}_{J,x}^T + \alpha^2 I_6\mathbf{\Phi}_I\mathbf{\Phi}_{J,x}^T)dx \tag{48}$$

$$[\mathbf{M}_b^{\psi\psi}]_{IJ} = \int_0^L (I_2 - 2\alpha I_4 + \alpha^2 I_6)\mathbf{\Phi}_I\mathbf{\Phi}_J^T dx \tag{49}$$

$$[\mathbf{C}_b^{ww}]_{IJ} = \int_0^L (\chi\mathbf{\Phi}_{I,x}\mathbf{\Phi}_{J,x}^T + \alpha^2 P_6\mathbf{\Phi}_{I,xx}\mathbf{\Phi}_{J,xx}^T)dx + 2Mv\mathbf{\Phi}_I(x_M)\mathbf{\Phi}_{J,x}^T(x_M)H(L-x_M) \tag{50}$$

$$[\mathbf{C}_b^{w\psi}]_{IJ} = \int_0^L (-\alpha P_4\mathbf{\Phi}_{I,xx}\mathbf{\Phi}_{J,x}^T + \chi\mathbf{\Phi}_{I,x}\mathbf{\Phi}_J^T + \alpha^2 P_6\mathbf{\Phi}_{I,xx}\mathbf{\Phi}_{J,x}^T)dx \tag{51}$$

$$[\mathbf{C}_b^{\psi w}]_{IJ} = \int_0^L (-\alpha P_4\mathbf{\Phi}_{I,x}\mathbf{\Phi}_{J,xx}^T + \chi\mathbf{\Phi}_I\mathbf{\Phi}_{J,x}^T + \alpha^2 P_6\mathbf{\Phi}_{I,x}\mathbf{\Phi}_{J,xx}^T)dx \tag{52}$$

$$[\mathbf{C}_b^{\psi\psi}]_{IJ} = \int_0^L [(P_2 - 2\alpha P_4 + \alpha^2 P_6)\mathbf{\Phi}_{I,x}\mathbf{\Phi}_{J,x}^T + \chi\mathbf{\Phi}_I\mathbf{\Phi}_J^T]dx \tag{53}$$

$$[\mathbf{K}_b^{ww}]_{IJ} = \int_0^L (\kappa\mathbf{\Phi}_{I,x}\mathbf{\Phi}_{J,x}^T + \alpha^2 J_6\mathbf{\Phi}_{I,xx}\mathbf{\Phi}_{J,xx}^T)dx + \int_{\Gamma_b} K_z\mathbf{\Phi}_I\mathbf{\Phi}_J^T d\Gamma + Mv^2\mathbf{\Phi}_I(x_M)\mathbf{\Phi}_{J,xx}^T(x_M)H(L-x_M) \tag{54}$$

$$[\mathbf{K}_b^{w\psi}]_{IJ} = \int_0^L (-\alpha J_4\mathbf{\Phi}_{I,xx}\mathbf{\Phi}_{J,x}^T + \kappa\mathbf{\Phi}_{I,x}\mathbf{\Phi}_J^T + \alpha^2 J_6\mathbf{\Phi}_{I,xx}\mathbf{\Phi}_{J,x}^T)dx \tag{55}$$

$$[\mathbf{K}_b^{\psi w}]_{IJ} = \int_0^L (-\alpha J_4\mathbf{\Phi}_{I,x}\Phi_{J,xx}^T + \kappa\mathbf{\Phi}_I\mathbf{\Phi}_{J,x}^T + \alpha^2 J_6\mathbf{\Phi}_{I,x}\mathbf{\Phi}_{J,xx}^T)dx \tag{56}$$

$$[\mathbf{K}_b^{\psi\psi}]_{IJ} = \int_0^L [(J_2 - 2\alpha J_4 + \alpha^2 J_6)\mathbf{\Phi}_{I,x}\mathbf{\Phi}_{J,x}^T + \kappa\mathbf{\Phi}_I\mathbf{\Phi}_J^T]dx \tag{57}$$

$$[\mathbf{f}_b^w]_I = Mg\mathbf{\Phi}_I(x_M)H(L-x_M) \tag{58}$$

It is obvious that the damping and stiffness matrices are not symmetric and time dependent. Therefore, a suitable scheme should be employed for solving the recent equations of motion in time domain. The generalized Newmark-β method [5] is utilized for required calculations at each time step. Without loss of generality, it is assumed that the beam is originally at rest; i.e., the initial conditions of the beam are $\mathbf{x}(0)=\mathbf{0}$ and $\dot{\mathbf{x}}(0)=\mathbf{0}$.

4 Numerical Simulations

4.1 Comparison of GMLSM Results With Those of Other Researchers. To investigate the proficiency of the proposed method in determining natural frequencies of the structure, the obtained results are verified with those of other researchers [18,19]. To this end, consider a single span simply supported Timoshenko beam with $k_b=0.833$. To compute the natural frequencies of the beam, one may take $\mathbf{x}(t)=\tilde{\mathbf{x}}_0 e^{i\omega t}$ in which $\tilde{\mathbf{x}}_0$ is the vector including the initial values of the discretized equations of motion. In the case of free vibration, by substituting this relation into the undamped equation of motion, one may arrive at

$$(-\omega^2\mathbf{M}_b + \mathbf{K}_b)\tilde{\mathbf{x}}_0 = \mathbf{0} \tag{59}$$

by solving this set of eigenvalue equations using an appropriate method, one can obtain eigenvalues (i.e., natural frequencies) and corresponding eigenvectors (i.e., related mode shapes). Moreover, the dimensionless frequency associated with the nth mode is defined as $\lambda_n=(\rho_b A_b\omega_n^2/E_b I_b)^{1/4} l_1$. In this work, for the case of stiff support ($K_z=\infty$), $K_z=10^9 E_b I_b/l_1^3$ is considered for proper modeling of the real problem. For numerical computation in this part via GMLSM, $4NS+1$ uniformly distributed particles, six Gaussian points within each computational cell, third-order base function, and weight function with influence domain radius of $3L/(NP-1)$ are taken into account. A preliminary analysis for the convergence check of the λ_n is carried out for a beam of rectangular cross section with $h/L=0.2$, and the results of the first ten dimensionless frequencies are given for the assumed Timoshenko beam in Table 1. The number of particles varies from 5 to 25 with an increment of 5. It is obvious that the convergence rate of the GMLSM is so fast in most of the frequencies such that for $NP=10$, the first ten dimensionless frequencies converge to four significant digits. For $NP\geq 20$, these values converge to six significant digits. Besides, the results of the proposed method with $NP=20$ are compared with those of Lee and Schultz [18] for different values of h/L, presented in Table 2. As it is clear, the computed results using GMLSM are in a reasonable good agreement with those of Lee and Schultz [18] based on pseudospectral method using 35 terms of Chebyshev polynomial. For instance, in the case of $h/L=0.2$, the results of GMLSM correspond to those of Lee and Schultz [18] with accuracy up to four significant digits.

In another comparison, the generated natural frequencies of a multispan Timoshenko beam are verified with the work of Lin and Chang [19]. In this case, consider an elastic simply supported Timoshenko beam, transversely constrained by an axial spring at its midspan. The related data for this example are as follows: $L=5$ m, $b=h=0.05$ m, $\rho_b=7800$ kg m^{-3}, $E_b=2.06\times 10^{11}$ N m^{-2}, $G_b=79\times 10^9$ N m^{-2}, and $\kappa_b=0.8497$. The predicted values of the proposed method for the first four natural frequencies are summarized in Table 3, where the results of Lin and Chang [19] are listed. As the results show for all cases, the predicted values of frequencies correspond to those of Lin and Chang [19] with the relative error lower than 0.5%.

4.2 Parametric Studies. Assessing the effects of the interested parameters related to the mathematical model of multispan viscoelastic beams under excitation of a moving mass, it would be convenient to define some normalized parameters. For this purpose, the maximum deflection plus the maximum negative and

Table 1 Convergence test of the dimensionless frequency parameter (λ_n) of the Timoshenko beam for different numbers of GMLSM particles (single span simply supported beam, $h/L = 0.2$)

Mode	$NP=5$	$NP=10$	$NP=15$	$NP=20$	$NP=25$
1	3.04541	3.04533	3.04533	3.04533	3.04533
2	5.67229	5.67156	5.67155	5.67154	5.67154
3	7.84735	7.83961	7.83953	7.83951	7.83951
4	9.80653	9.65740	9.65714	9.65708	9.65708
5	11.72863	11.22273	11.22219	11.22203	11.22204
6	13.03233	12.60361	12.60254	12.60221	12.60221
7	13.44427	13.03233	13.03231	13.03230	13.03230
8	14.16642	13.44427	13.44426	13.44425	13.44425
9	14.43845	13.84807	13.84390	13.84330	13.84330
10	15.67197	14.43774	14.43776	14.43774	14.43774

positive bending moments are normalized according to the appropriate maximum parameter values generated by an equivalent statically applied point load over the corresponding elastic thin beam, i.e., $W_{\max,\text{st}}$, $M^-_{\max,\text{st}}$, and $M^+_{\max,\text{st}}$. These parameters are exemplified in Table 4 for EBs up to six spans. Moreover, the nondimensional slenderness, velocity, and mass parameters are assumed to be like $\lambda = l_1/r$, $V_N = v/v'$ [4], and $M_N = M/\rho_b A_b l_1$, respectively, where $v' = \pi/l_1 \sqrt{E_b I_b/\rho_b A_b}$ and r is the gyration radius of the beam cross section about its neutral axis. The geometrical and material properties of the beam are considered as $l_1 = 10$ m, $E_b = 2.1\times 10^{11}$ N m^{-2}, $G_b = 8.0769\times 10^{10}$ N m^{-2}, $b = 0.1$ m, $h = \sqrt{12}r$, $k_b = 0.833$, and $\rho_b = 7800$ kg m^{-3}.

In Figs. 2–5, the variation in normalized design parameters in terms of span number, moving mass velocity, different values of beam slenderness, and material relaxation rates is depicted. As it may be observed through Figs. 2(*a*)–2(*c*) and 5(*a*)–5(*c*), for deep beams ($\lambda = 10$) and high values of moving mass velocities (e.g., $V_N = 0.8$), increasing the span number leads to higher differences in design parameter values of EB and those of TB and HOB. As the beam slenderness increases, the results of different beam theories approach the same values regardless of span number as well as moving mass velocity. Also, for high levels of moving mass velocity, the design parameter values increase as the span number increases, specifically for low values of material relaxation rate (Figs. 2 and 3). In contrast to the abovementioned findings, for $V_N \leq 0.5$, the design parameter values do not change appreciably, irrespective of the considered beam theory as well as the span number. Furthermore, the differences between the results of the assumed beam theories and the design parameter values diminish as the material relaxation rate increases (Figs. 2–5).

Table 2 Verification of the first 15 dimensionless frequencies (λ_n) in the present study for a simply supported Timoshenko beam with the results of Lee and Schultz [18]

	$h/L=0.02$		$h/L=0.05$		$h/L=0.1$		$h/L=0.2$	
Mode	LS[a]	Present work	LS	Present work	LS	Present work	LS	Present work
1	3.1405	3.1406	3.1350	3.1350	3.1157	3.1157	3.0453	3.0453
2	6.2747	6.2747	6.2314	6.2314	6.0907	6.0907	5.6716	5.6715
3	9.3963	9.3963	9.2554	9.2554	8.8405	8.8405	7.8395	7.8395
4	12.4994	12.4996	12.1813	12.1814	11.3431	11.3431	9.6571	9.6571
5	15.5784	15.5792	14.9926	14.9928	13.6132	13.6132	11.2220	11.2220
6	18.6282	18.6300	17.6810	17.6815	15.6790	15.6792	12.6022	12.6022
7	21.6443	21.6475	20.2447	20.2455	17.5705	17.5709	13.0323	13.0323
8	24.6227	24.6273	22.6862	22.6876	19.3142	19.3148	13.4443	13.4443
9	27.5599	27.5662	25.0111	25.0132	20.9325	20.9336	13.8433	13.8433
10	30.4533	30.4615	27.2263	27.2293	22.4441	22.4456	14.4378	14.4377
11	33.3006	33.3113	29.3394	29.3436	23.8639	23.8660	14.9766	14.9769
12	36.1001	36.1141	31.3581	31.3637	25.2044	25.2074	15.6676	15.6676
13	38.8507	38.8687	33.2896	33.2973	26.0647	26.0646	16.0241	16.0247
14	41.5517	41.5734	35.1410	35.1509	26.2814	26.2814	16.9584	16.9584
15	44.2026	44.2316	36.9186	36.9318	26.4758	26.4799	17.0019	17.0027

[a]Lee and Schultz (LS) [18].

Table 3 Comparison of the lowest four natural frequencies in a two-span Timoshenko beam analyzed by GMLSM with the results of Lin and Chang [19] for various values of intermediate spring stiffness

Frequency (Hz)	$K_z = 10{,}000{,}000$ N/m		$K_z = 10{,}000{,}000$ N/m		$K_z = \infty$	
$f_n = \omega_n/(2\pi)$	LC[a]	Present work	LC	Present work	LC	Present work
f_1	18.738	18.980	18.738	18.976	18.614	18.917
f_2	28.004	27.907	29.143	29.040	29.122	29.177
f_3	74.802	75.047	74.802	74.576	74.566	74.495
f_4	80.317	79.690	93.306	92.529	94.515	93.833

[a]Lin and Chang (LC) [19].

Table 4 The values of $W_{\max,st}$, $M^{-}_{\max,st}$, and $M^{+}_{\max,st}$ for elastic multispan Euler–Bernoulli beams under statically applied point load via GMLSM

NS	1	2	3	4	5	6
$\bar{W}_{st}$	0.02077	0.01506	0.01459	0.01456	0.01456	0.01456
$\bar{M}^{-}_{st}$	-	−0.09782	−0.09982	−0.10019	−0.10022	−0.10023
$\bar{M}^{+}_{st}$	0.24418	0.18573	0.17860	0.17835	0.17834	0.17833

Note that $\bar{W}_{st}=W_{\max,st}/(Mgl_1^3/E_bI_b)$, $\bar{M}^{-}_{st}=M^{-}_{\max,st}/(Mgl_1)$, and $\bar{M}^{+}_{st}=M^{+}_{\max,st}/(Mgl_1)$.

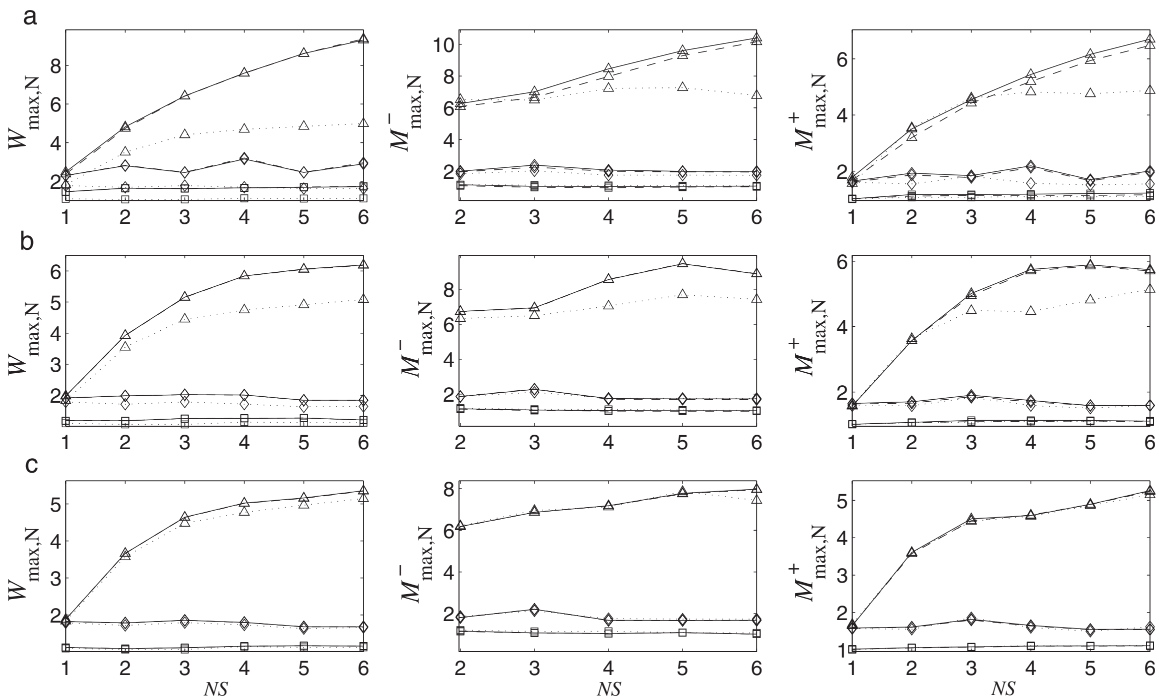

Fig. 2 Variation in the normalized design parameters in terms of span number for $\lambda_x=\lambda_z=0.00001$: (*a*) $\lambda=10$, (*b*) $\lambda=20$, and (*c*) $\lambda=40$ ((□) $V_N=0.2$, (◇) $V_N=0.5$, and (△) $V_N=0.8$; (...) EBT, (− −) TBT, and (—) HOBT; $M_N=0.15$)

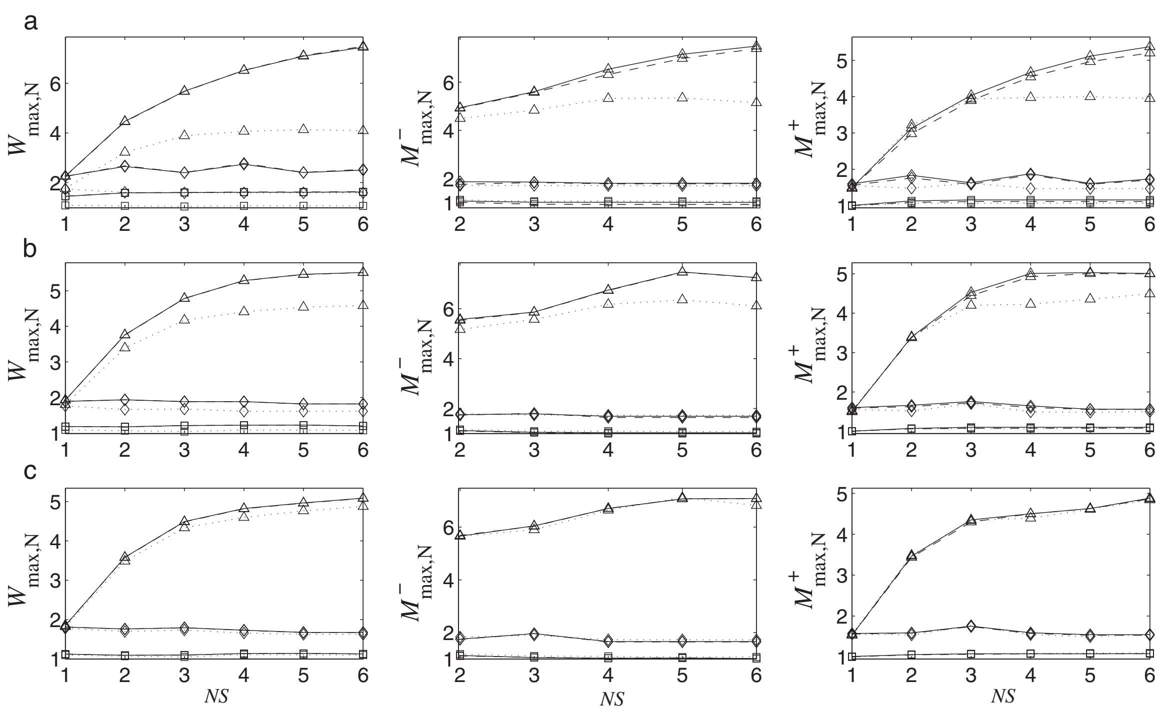

Fig. 3 Variation in the normalized design parameters in terms of span number for $\lambda_x=\lambda_z=0.0001$: (*a*) $\lambda=10$, (*b*) $\lambda=20$, and (*c*) $\lambda=40$ ((□) $V_N=0.2$, (◇) $V_N=0.5$, and (△) $V_N=0.8$; (...) EBT,(− −) TBT, and (—) HOBT; $M_N=0.15$)

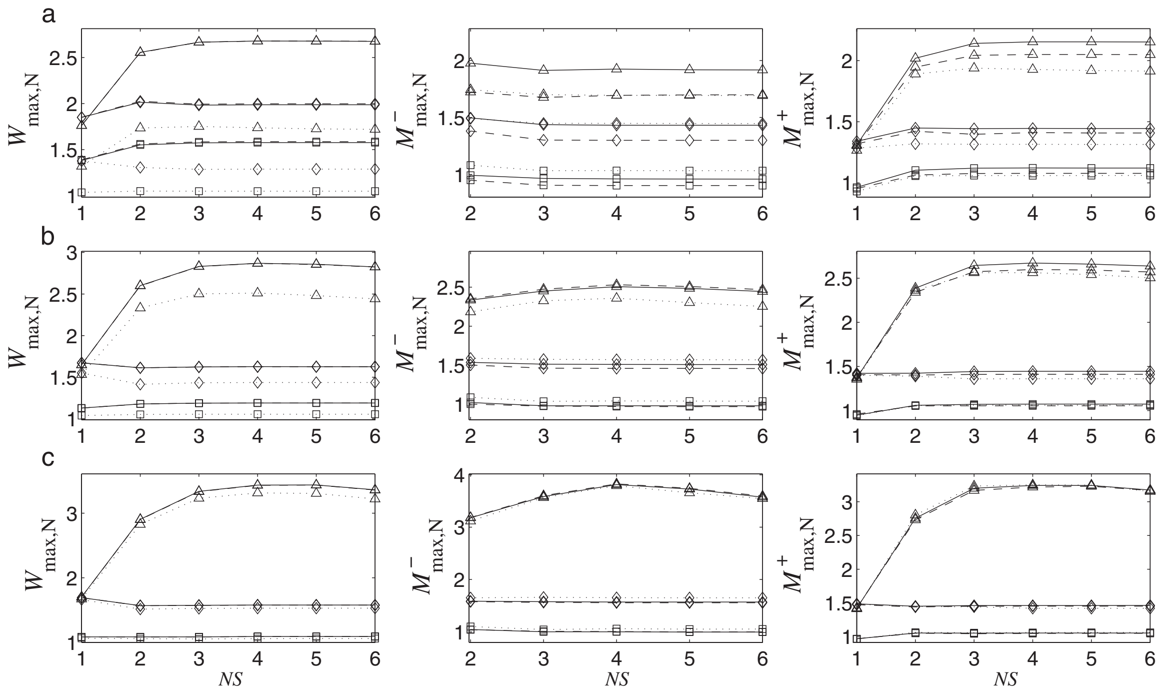

Fig. 4 Variation in the normalized design parameters in terms of span number for $\lambda_x=\lambda_z=0.001$: (*a*) $\lambda=10$, (*b*) $\lambda=20$, and (*c*) $\lambda=40$ ((□) $V_N=0.2$, (◇) $V_N=0.5$, and (△) $V_N=0.8$; (...) EBT, (− −) TBT, and (—) HOBT; $M_N=0.15$)

On the other hand, an important phenomenon in such a loading is the onset of the moving mass separation from the base beam during the course of vibration [20]. The possibility of this phenomenon could be addressed by checking the sign of the contact force between the moving mass and the base beam, which is defined as

$$F=[Mg-M(\ddot{w}+2v\dot{w}_{,x}+v^2w_{,xx})]_{x=x_M} \tag{60}$$

the onset of separation occurs as the sign of F changes from positive to negative. Assuming the normalized value of the contact force as $F_N=F/Mg$, the variation in the extremum values of this

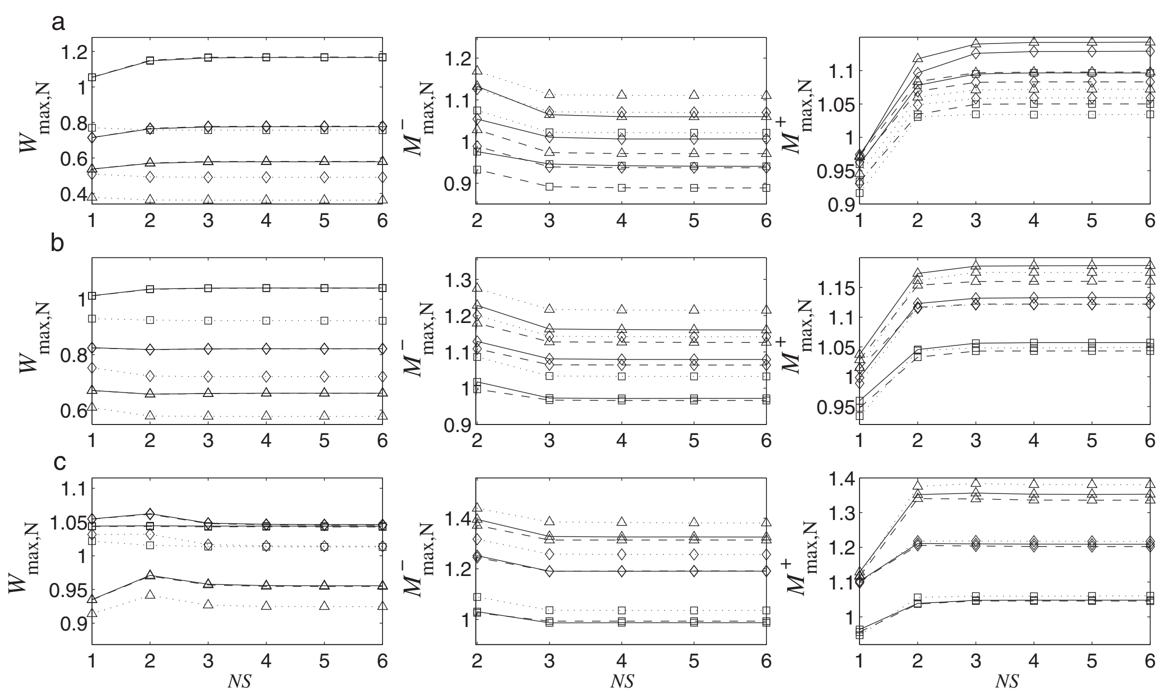

Fig. 5 Variation in the normalized design parameters in terms of span number for $\lambda_x=\lambda_z=0.01$: (*a*) $\lambda=10$, (*b*) $\lambda=20$, and (*c*) $\lambda=40$ ((□) $V_N=0.2$, (◇) $V_N=0.5$, and (△) $V_N=0.8$; (...) EBT, (− −) TBT, and (—) HOBT; $M_N=0.15$)

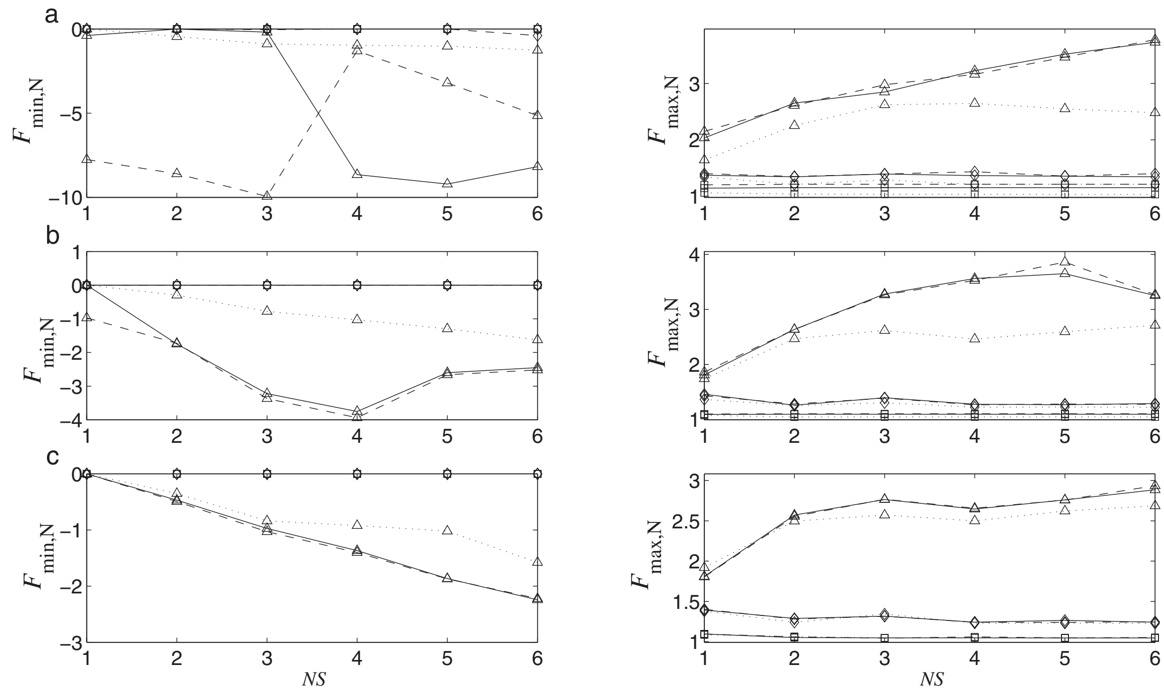

Fig. 6 Variation in the normalized values of minimum and maximum contact forces in terms of span number for $\lambda_x=\lambda_z=0.00001$: (*a*) $\lambda=10$, (*b*) $\lambda=20$, and (*c*) $\lambda=40$ ((□) $V_N=0.2$, (◇) $V_N=0.5$, and (△) $V_N=0.8$; (...) EBT, (− −) TBT, and (—) HOBT; $M_N=0.15$)

parameter in terms of *NS*, λ_x, V_N, and λ is plotted in Figs. 6–9. As it could be observed from Fig. 6(*a*), for high moving mass velocities, the results of normalized minimum contact force in deep beams are obviously distinct for different assumed beam theories. This is not the case for the normalized maximum contact force in TB and HOB, even for high moving mass velocities. As the base beam slenderness increases, the differences between the results of various beam theories decrease (see Fig. 6). Moreover, irrespective of the assumed beam theory, the possibility of mass separation magnifies as the beam span number increases. Expectedly, as the viscosity of the base beam increases, there would be a decrease in the absolute value of the normalized minimum contact force. It implies that the higher the beam viscosity, the lower the possibility of mass separation (Figs. 6–9). Another significant

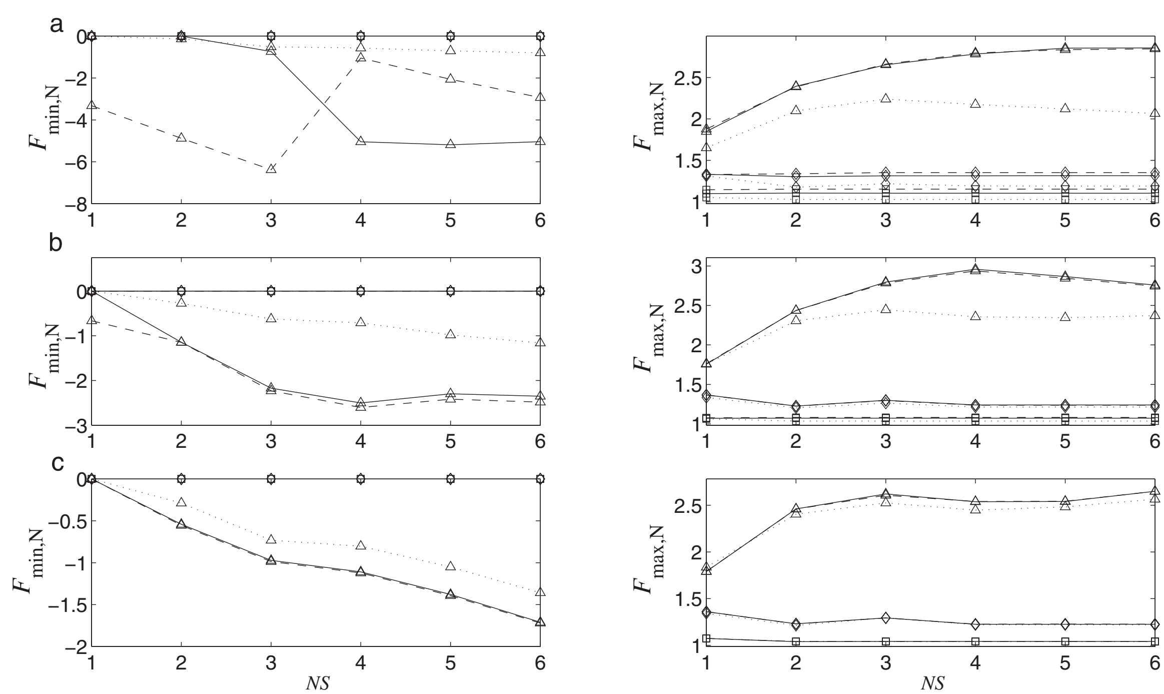

Fig. 7 Variation in the normalized values of minimum and maximum contact forces in terms of span number for $\lambda_x=\lambda_z=0.0001$: (*a*) $\lambda=10$, (*b*) $\lambda=20$, and (*c*) $\lambda=40$ ((□) $V_N=0.2$, (◇) $V_N=0.5$, and (△) $V_N=0.8$; (...) EBT, (− −) TBT, and (—) HOBT; $M_N=0.15$)

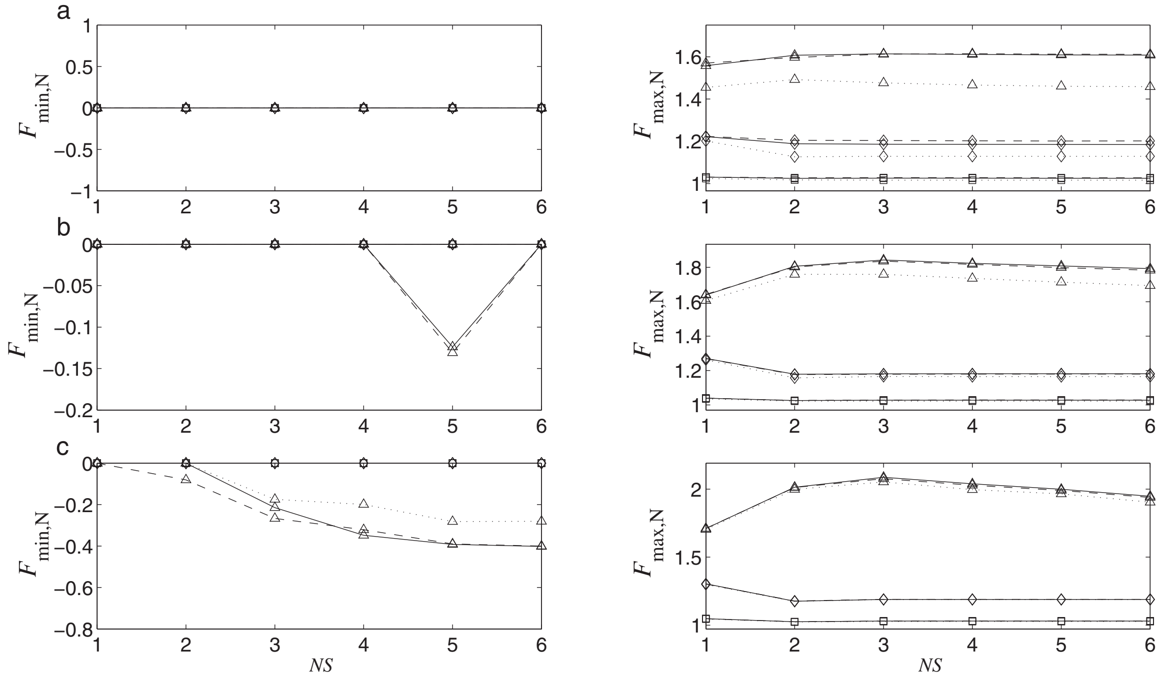

Fig. 8 Variation in the normalized values of minimum and maximum contact forces in terms of span number for $\lambda_x=\lambda_z=0.001$: (*a*) $\lambda=10$, (*b*) $\lambda=20$, and (*c*) $\lambda=40$ (($\square$) $V_N=0.2$, ($\diamond$) $V_N=0.5$, ($\triangle$) $V_N=0.8$; (...) EBT, (– –) TBT, and (—) HOBT; $M_N=0.15$)

point is a correlation between the normalized maximum contact forces of different beam theories with the results of normalized design parameters. This could be readily noticed by a simple comparison of Figs. 6–9 with Figs. 2–5.

As a general conclusion based on Figs. 2–9, the appropriate beam theory should be selected according to the beam slenderness for any dynamic analysis. Hence, to investigate the effect of mass weight and velocity of the moving mass on dynamic behavior of multispan beams, EBT, TBT, and HOBT are adopted for $\lambda=40$, $\lambda=20$, and $\lambda=10$, correspondingly (Figs. 10–12). As it is seen in Fig. 10(*a*), the inertial effects of the moving mass are not remarkable for low levels of moving mass velocity ($V_N \leq 0.2$). In such velocities, the values of design parameters are almost independent of the beam span number. This fact could be observed in deeper

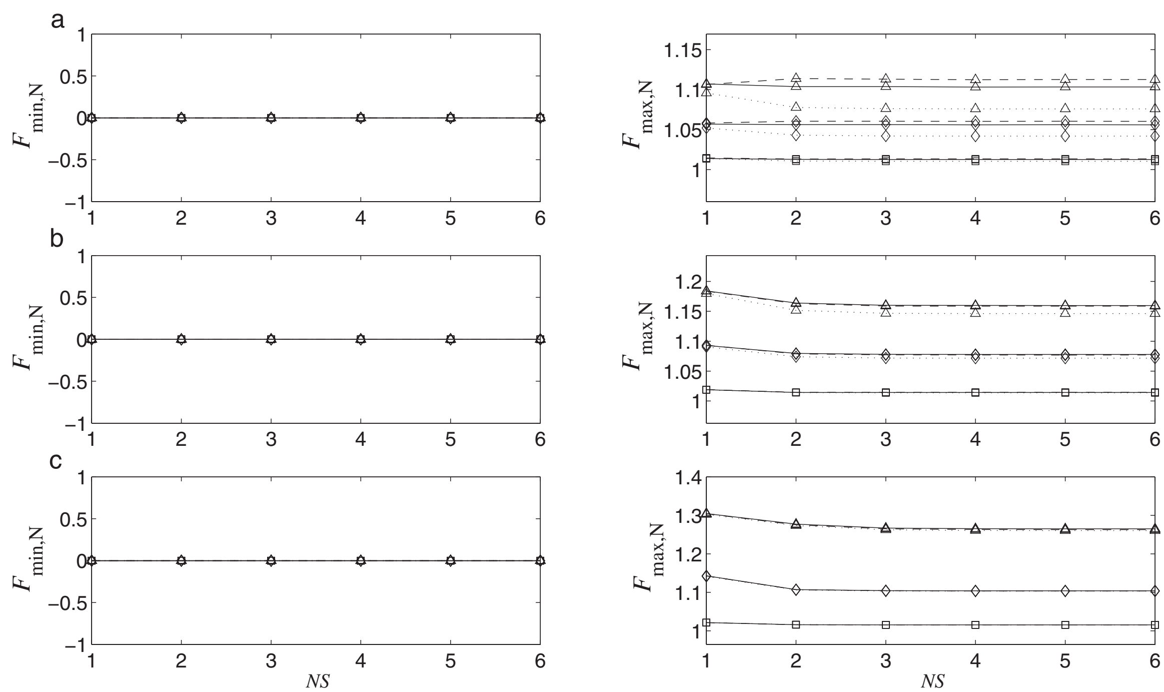

Fig. 9 Variation in the normalized values of minimum and maximum contact forces in terms of span number for $\lambda_x=\lambda_z=0.01$: (*a*) $\lambda=10$, (*b*) $\lambda=20$, and (*c*) $\lambda=40$ (($\square$) $V_N=0.2$, ($\diamond$) $V_N=0.5$, ($\triangle$) $V_N=0.8$; (...) EBT, (– –) TBT, and (—) HOBT; $M_N=0.15$)

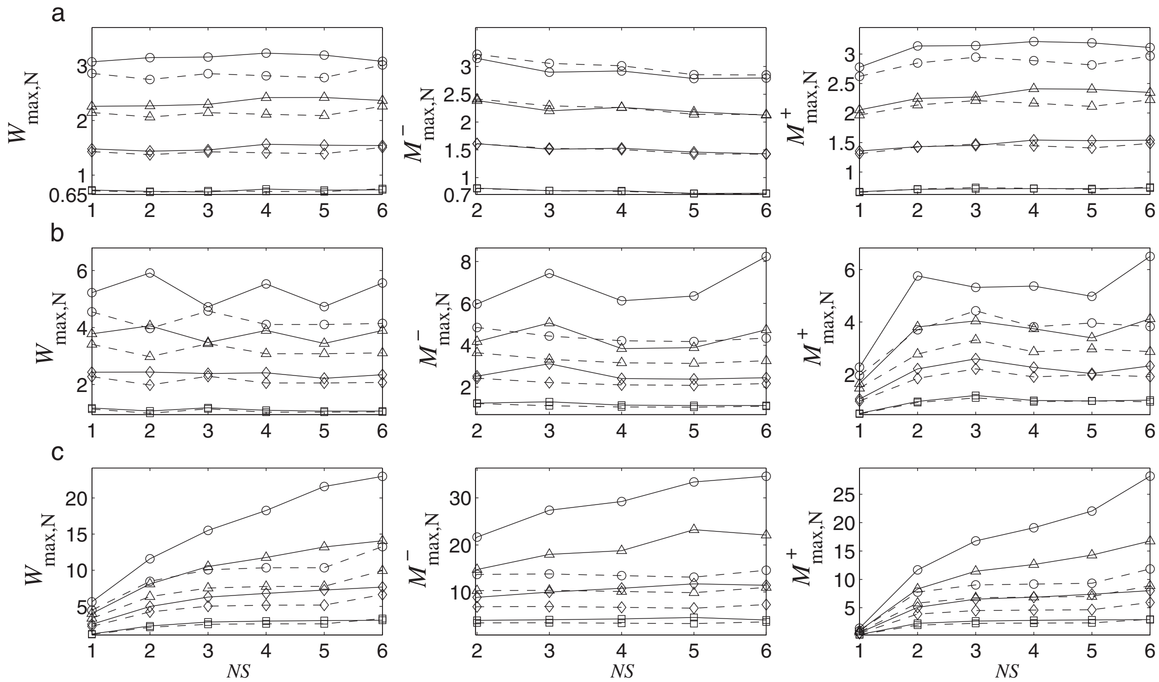

Fig. 10 Variation in the normalized design parameters in terms of span number based on EBT for $\lambda=40$ and $\lambda_x=0.00001$: (*a*) $V_N=0.2$, (*b*) $V_N=0.5$, and (*c*) $V_N=0.8$ ((□) $M_N=0.1$, (◇) $M_N=0.2$, (△) $M_N=0.3$, and (○) $M_N=0.4$; (– –) moving load and (—) moving mass)

beams for $NS\geq 2$ either (Figs. 11(*a*) and 12(*a*)). In the case of $V_N=0.5$ (Figs. 10(*b*)–12(*b*)), the inertial effects of moving mass are more apparent, and there would be a slight dependency of the design parameters to the beam span number. For high moving mass velocities ($V_N\geq 0.5$), not only the results of moving mass are totally distinct of those of moving loads but also the design parameter values increase with the beam span number, especially for high values of moving mass weight (see Fig. 10(*c*)). This fact could also be detected in deeper beams ($\lambda=10,20$) (see Figs. 11(*c*) and 12(*c*)).

5 Conclusion

A comprehensive numerical parametric study was conducted on the design parameters of multispan viscoelastic Timoshenko and

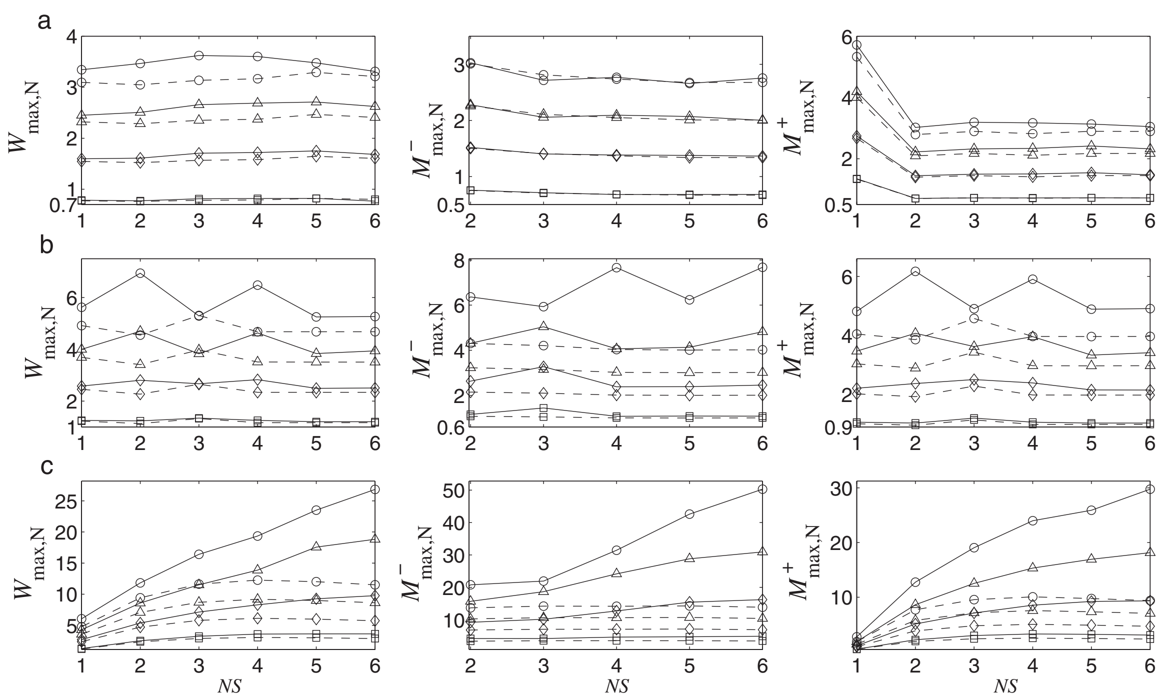

Fig. 11 Variation in the normalized design parameters in terms of span number based on TBT for $\lambda=20$ and $\lambda_x=\lambda_z=0.00001$: (a) $V_N=0.2$, (b) $V_N=0.5$, and (c) $V_N=0.8$ ((□) $M_N=0.1$, (◇) $M_N=0.2$, (△) $M_N=0.3$, and (○) $M_N=0.4$; (– –) moving load and (—) moving mass)

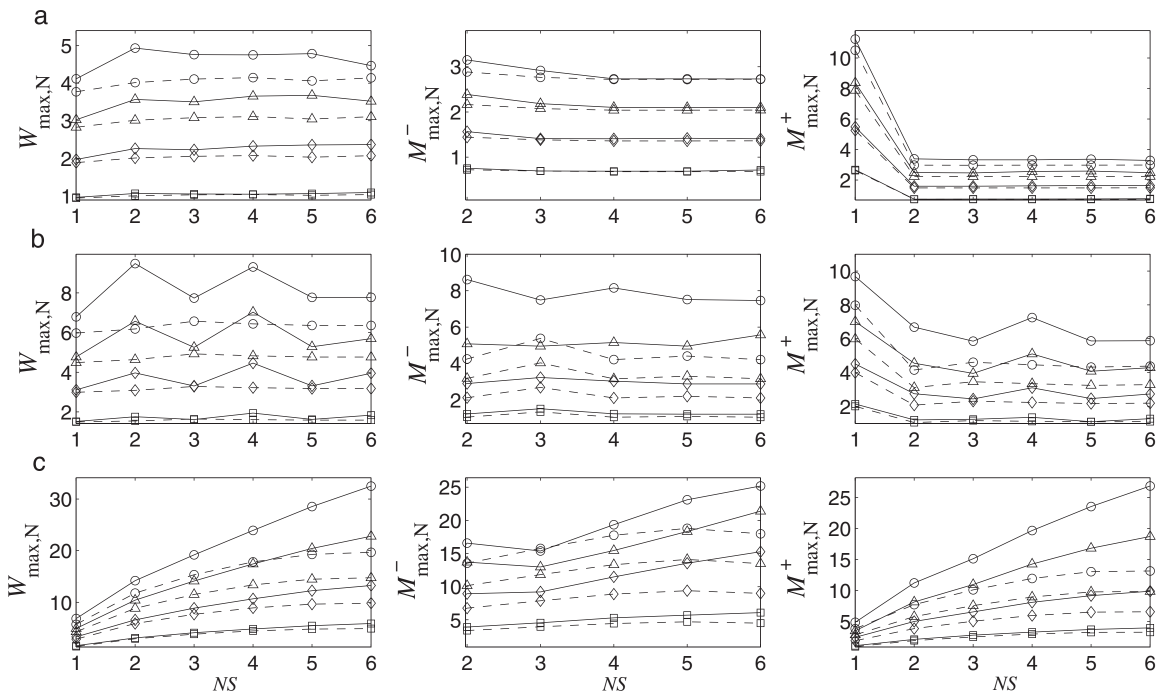

Fig. 12 Variation in the normalized design parameters in terms of span number based on HOBT for $\lambda=10$ and $\lambda_x=\lambda_z=0.00001$: (*a*) $V_N=0.2$, (*b*) $V_N=0.5$, and (*c*) $V_N=0.8$ ((□) $M_N=0.1$, (◇) $M_N=0.2$, (△) $M_N=0.3$, and (○) $M_N=0.4$; (− −) moving load and (—) moving mass)

higher-order beams under excitation of a moving mass by utilizing GMLSM. In this regard, the maximum values of deflection as well as maximum negative and positive values of bending moment were considered as the crucial design parameters. For using Lagrange's equations, the unknown parameters of the problem were discretized according to the so-called meshless numerical method, and then the generalized Newmark-β scheme was employed for solving discrete equations of motion in time domain. The validity of the proposed numerical method was confirmed by verifying the obtained results with those of other researchers for the special cases of the studied problem. The effects of moving mass weight and velocity, material relaxation rate, slenderness, and span number of the base beam on the design parameters were studied for multispan viscoelastic Euler–Bernoulli, Timoshenko, and higher-order beams. The results manifested that for low values of beam slenderness, the EBT or even TBT could not precisely predict the real dynamic behavior of the multispan viscoelastic beam. As a result, higher beam span number would result in higher difference between the predicted values of design parameters in shear deformable beams and those of thin beams. Moreover, the results demonstrated that the values of design parameters as well as the inertial effects of the moving mass increase as the beam span number increases, specifically for high levels of moving mass velocity and low values of material relaxation rate. Furthermore, for all beam theories, it was indicated that the possibility of mass separation moves to greater extent as the beam span number increases, particularly for low values of material relaxation rate.

References

[1] Frýba, L., 1999, *Vibration of Solids and Structures Under Moving Loads*, Thomas Telford, London.

[2] Visweswara Rao, G., 2000, "Linear Dynamics of an Elastic Beam Under Moving Loads," ASME J. Vibr. Acoust., **122**(3), pp. 281–289.

[3] Bilello, C., Bergman, L. A., and Kuchma, D., 2004, "Experimental Investigation of a Small-Scale Bridge Model Under a Moving Mass," J. Struct. Eng., **130**(5), pp. 799–804.

[4] Nikkhoo, A., Rofooei, F. R., and Shadnam, M. R., 2007, "Dynamic Behavior and Modal Control of Beams Under Moving Mass," J. Sound Vib., **306**(3–5), pp. 712–724.

[5] Kiani, K., Nikkhoo, A., and Mehri, B., 2009, "Prediction Capabilities of Classical and Shear Deformable Beam Models Excited by a Moving Mass," J. Sound Vib., **320**(3), pp. 632–648.

[6] Lee, H. P., 1996, "The Dynamic Response of a Timoshenko Beam Subjected to a Moving Mass," J. Sound Vib., **198**(2), pp. 249–256.

[7] Wu, J. S., and Dai, C. W., 1987, "Dynamic Responses of Multispan Nonuniform Beam Due to Moving Loads," J. Struct. Eng., **113**(3), pp. 458–474.

[8] Lee, H. P., 1994, "Dynamic Response of a Beam With Intermediate Point Constraints Subjected to a Moving Load," J. Sound Vib., **171**(3), pp. 361–368.

[9] Chatterjee, P. K., Datta, T. K., and Surana, C. S., 1994, "Vibration of Continuous Bridges Under Moving Vehicles," J. Sound Vib., **169**(5), pp. 619–632.

[10] Henchi, K., Fafard, M., Dhatt, G., and Talbot, M., 1997, "Dynamic Behaviour of Multispan Beams Under Moving Loads," J. Sound Vib., **199**(1), pp. 33–50.

[11] Ichikawa, M., Miyakawa, Y., and Matsuda, A., 2000, "Vibration Analysis of the Continuous Beam Subjected to a Moving Mass," J. Sound Vib., **230**(3), pp. 493–506.

[12] Toshiaki, I., and Kenichi, H., 2000, "Transfer Matrix Analysis of Dynamic Responses of Multispan Beam Under Moving Loads With Spring and Damping," Trans. Jpn. Soc. Mech. Eng., Ser. A, **66**(647), pp. 1377–1384.

[13] Wang, R. T., 1997, "Vibration of Multispan Timoshenko Beams to a Moving Force," J. Sound Vib., **207**(5), pp. 731–742.

[14] Wang, R. T., and Tsu, J. T., 2001, "Out-of-Plane Vibration of a Multi-Span Timoshenko Curved Beam Due to a Moving Load Including the Warping Inertia of the Beam," J. Chin. Inst. Eng., **24**(4), pp. 407–417.

[15] Zhu, X. Q., and Law, S. S., 1999, "Moving Forces Identification on a Multispan Continuous Bridge," J. Sound Vib., **228**(2), pp. 377–396.

[16] Atluri, S. N., Cho, Y. J., and Kim, H. G., 1999, "Analysis of Thin Beams Using the Meshless Local Petrov–Galerkin Method With Generalized Moving Least Squares Interpolations," Comput. Mech., **24**(5), pp. 334–347.

[17] Reddy, J. N., 1997, *Mechanics of Laminated Composite Plates: Theory and Analysis*, CRC, Boca Raton, FL.

[18] Lee, J., and Schultz, W. W., 2004, "Eigenvalue Analysis of Timoshenko Beams and Axisymmetric Mindlin Plates by the Pseudospectral Method," J. Sound Vib., **269**, pp. 609–621.

[19] Lin, H. P., and Chang, S. C., 2005, "Free Vibration Analysis of Multi-Span Beams With Intermediate Flexible Constraints," J. Sound Vib., **281**(1–2), pp. 155–169.

[20] Lee, U., 1996, "Revisiting the Moving Mass Problem: Onset of Separation Between the Mass and Beam," ASME J. Vibr. Acoust., **118**(3), pp. 516–521.